PHYSICAL REVIEW B **74**, 041302(R) (2006)

Experimental realization of a ballistic spin interferometer based on the Rashba effect using a nanolithographically defined square loop array

Takaaki Koga,[1,2,3,*] Yoshiaki Sekine,[2] and Junsaku Nitta[2,3,†]
[1] *PRESTO, Japan Science and Technology Agency, 4-1-8, Honchou, Kawaguchi, Saitama 332-0012, Japan*
[2] *NTT Basic Research Laboratories, NTT Corporation, 3-1, Morinosato-Wakamiya, Atsugi, Kanagawa 243-0198, Japan*
[3] *CREST, Japan Science and Technology Agency, 4-1-8, Honchou, Kawaguchi, Saitama 332-0012, Japan*

(Received 13 April 2006; published 14 July 2006)

We succeeded in observing gate-controlled electron spin interference in nanolithographically defined square loop arrays that were fabricated in $\mathrm{In_{0.52}Al_{0.48}As/In_{0.53}Ga_{0.47}As/In_{0.52}Al_{0.48}As}$ quantum wells (QWs). In this experiment, we demonstrated electron spin precession in ballistic channels within the QW that is caused by the Rashba effect. It turned out that the spin precession angle θ was gate controllable by more than 0.75π for a length of 1.5 μm. Thus, the demonstration of the large controllability of θ by the applied gate voltage was carried out in a more direct way using spin interference of an electron wave function than the conventional beating analysis of the Shubnikov–de Haas oscillations.

DOI: 10.1103/PhysRevB.74.041302 PACS number(s): 73.63.Hs, 71.70.Ej, 73.20.Fz, 73.23.Ad

Exploitation of the spin degree of freedom for the conduction carriers provides a key strategy for finding new functional devices in semiconductor spintronics.[1–6] A promising approach for manipulating spins in semiconductors is the utilization of spin-orbit (SO) interactions. In this regard, lifting of the spin degeneracy in the conduction (or valence) band due to the structural inversion asymmetry in particular is called the "Rashba effect,"[7,8] the magnitude of which can be controlled by the applied gate voltage and/or the specific design of the sample heterostructures.[9,10]

Recently, we proposed a ballistic spin interferometer (SI) using a square loop (SL) geometry, where an electron spin rotates by an angle θ due to the Rashba effect as it travels along a side of the SL ballistically.[11] In a simple SI model, an incident electron wave is split by a "hypothetical" beam splitter into two partial waves, and each of these follows a SL path in the clockwise and counterclockwise directions, respectively (see Fig. 1 in Ref. 11). Then they interfere with each other when they come back to the incident point at the beam splitter. As a consequence, the incident electron can either scatter back to the incident path (called "path 1") or emerge on the other path (called "path 2"). The backscattering probability to path 1 (P_{back}) for a spin-unpolarized incident electron is given by[11]

$$P_{\mathrm{back}} = \frac{1}{2} + \frac{1}{4}(\cos^4\theta + 4\cos\theta\sin^2\theta + \cos 2\theta)\cos\phi$$
$$\equiv \frac{1}{2} + A(\theta)\cos\phi, \qquad (1)$$

where ϕ is the quantum mechanical phase due to the vector potential responsible for the magnetic field $\mathbf{B}$ piercing the SL ($\phi=2eBL^2/\hbar$, L being the side length of the SL) and θ is the spin precession angle due to the Rashba effect ($\theta=2\alpha m^* L/\hbar^2$, α and m^* being the Rashba SO coupling constant and the electron effective mass, respectively[10]). $A(\theta)$ is an oscillating function of θ with a maximum (minimum) value of $1/2(-1/2)$ at $\theta=0, \pm\pi, \pm 2\pi$ ($\theta\approx\pm 2.0$ and ± 4.28) (see Fig. 2 in Ref. 11), where $A(\theta)$ becomes zero for $\theta\approx\pm 0.4245\pi$, $\pm 0.822\pi$, and $\pm 1.178\pi$. We note that $A(\theta)$ corresponds to the amplitude of the "experimentally observable" Al'tshuler-Aronov-Spivak- (AAS-) type oscillations of electric resistance as a result of averaging out all kinds of random processes including Elliott-Yafet, D'yakonov-Perel', and hyperfine interactions with nuclear spins by arraying the loops.[12] Equation (1) predicts that the amplitude of the AAS oscillation should be modulated as a function of θ and varnish at $\theta\approx\pm 0.4245\pi$, $\pm 0.822\pi$, and $\pm 1.178\pi$. Experimentally, the value of θ can be controlled by the applied gate voltage V_{g} through the variation of α. A noteworthy feature here, again, is the fact that $A(\theta)$ oscillates between positive and negative values coherently with increasing strength of the SO interaction, which is represented by θ, whereas, in earlier experiments using arrays of metal rings,[13] the strength of the SO interaction in the system was controlled by varying the densities of heavy-ion impurities that act as SO scatterers. In the latter case the phases of AAS oscillations at $B=0$ flip only once on increasing the strength of the SO scattering.

In this Rapid communication, we present an experimental demonstration of the SI using nanolithographically defined SL arrays in epitaxially grown (001) $\mathrm{In_{0.52}Al_{0.48}As/In_{0.53}Ga_{0.47}As/In_{0.52}Al_{0.48}As}$ quantum wells (QWs). We use the same epiwafers grown by metal-organic chemical vapor deposition as those we used for the weak antilocalization (WAL) study previously.[10] We first exploit the electron beam lithography (EBL) and subsequently electron cyclotron resonance (ECR) plasma etching techniques to define an array of SLs in an area of 150×200 $\mu\mathrm{m}^2$. We then use the photolithography and wet etching techniques to form a Hall bar mesa of the size of 125×250 $\mu\mathrm{m}^2$ over the SL array regions. In this way, the area of the final SL array region in the Hall bar mesa is 125×200 $\mu\mathrm{m}^2$ [see Fig. 1(b)]. These samples have a gate electrode (Au) covering the entire Hall bar, using a 100-nm-thick $\mathrm{SiO_2}$ layer as a gate insulator, which makes it possible to control the sheet carrier density N_{S} and the Rashba spin-orbit parameter α by the applied gate voltage V_{g}. We estimate the nonuniformity of the thickness of the $\mathrm{SiO_2}$ layer to be at most ±5% across the entire mesa, which

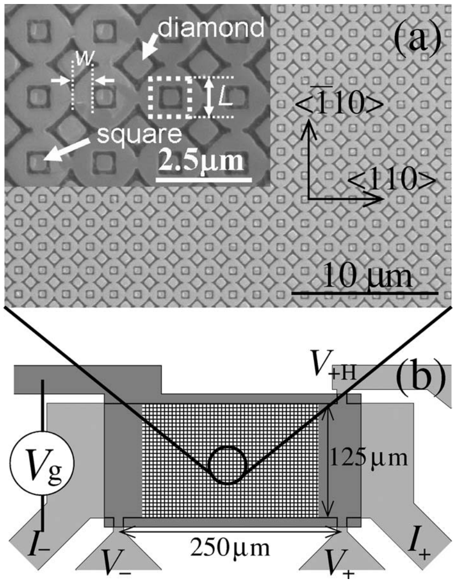

FIG. 1. (a) SEM micrographs of the nanolithographically defined square loop array (L=1.2 μm). A two-dimensional electron gas exists in the lighter-color regions. (b) Schematic diagram for the Hall bar sample used in the present experiment.

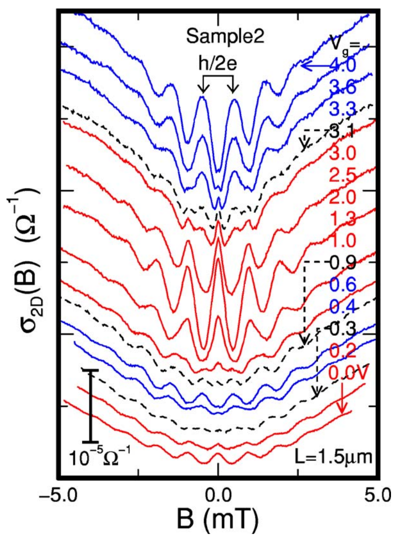

FIG. 2. (Color online) Gate-voltage dependence of the electric sheet conductivities σ_{2D} as a function of the magnetic field B for a square loop (SL) array sample (L=1.5 μm) fabricated using the sample 2 epiwafer in Ref. 10. The plotted curves are shifted along y axis for the ease of comparison. The magnitudes of σ_{2D} at B=0 range from 3.7×10^{-4} Ω^{-1} (for V_g=0.0 V) to 10.3×10^{-4} Ω^{-1} (for V_g=4.0 V). The range of B (ΔB) that corresponds to the magnetic flux half quanta piercing the SL ($\Delta B\times L^2=h/2e$) is indicated by "$h/2e$" in the figure.

typically can be converted to ±3% in the value of α. We note that all the measurements were carried out at T=0.3 K using a ^{3}He cryostat, exploiting the conventional ac lock-in technique. When the electric sheet conductivities σ_{2D} of these samples were measured [using the electrodes labeled by I_+, I_-, V_+ and V_- in Fig. 1(b)] as a function of B (**B** perpendicular to the sample surface) for a given V_g [denoted as $\sigma_{2D}(B)$], the Hall voltages were also monitored using the electrodes labeled by V_+ and V_{+H} to obtain the N_S value at the same V_g. We then investigate the amplitude of the AAS oscillations at B=0 [denoted as $\Delta\sigma_{2D}(B=0)$], as a function of V_g (equivalently N_S), to test the prediction of the SI.[11]

Examples of the scanning electron micrograph (SEM) of the SL pattern used in the present experiment are shown in Fig. 1(a). We note that electrons exist in the relatively lighter regions of the picture. The relatively darker lines and curves that define the diamond and square shapes in the inset of Fig. 1(a) are the ditches created by the ECR plasma etching. We note that electrons exist within these diamond- and square-shaped islands. However, these islands do not contribute to the electron transport, since they are not electrically connected to one another. We sketch a SL path for the spin interference by the dotted white square in the inset of Fig. 1(a), where electrons will be localized if the type of spin interference is constructive. The width W of the SL path [defined in Fig. 1(a)] was 0.5 μm throughout the present experiment. Note that these SLs are electrically connected with the neighboring SLs and contribute to the electric conductivity for the whole Hall bar.

Shown in Fig. 2 is the gate voltage (V_g) dependence of $\sigma_{2D}(B)$ for a SL array sample (L=1.5 μm) that was fabricated using the sample 2 epiwafer in Ref. 10. Here, we clearly see AAS oscillations, whose period (ΔB) is given by $h/2eL^2$. We note that the observed AAS oscillations decay rather rapidly with increasing B due to the exisitence of multiple channels within a finite channel width W. We also note, as predicted theoretically, that as the value of V_g is increased from 0.0 V, the peak feature in $\sigma_{2D}(B)$ at B=0 becomes a dip across V_g=0.3 V [dashed $\sigma_{2D}(B)$ curve]. Then, the dip feature becomes a peak for $V_g>0.9$ V [also indicated by another dashed $\sigma_{2D}(B)$ curve]. Finally the peak feature again becomes a dip for $V_g>3.1$ V. Thus the amplitude of the AAS oscillations at B=0 oscillates as a function of V_g as predicted in Eq. (1). It is noted that the elastic mean free path for electrons, ℓ_e, is typically 1.2 μm for V_g=0.0 V (N_S $=1.7\times10^{12}$ cm^{-2}) in Fig. 2, and becomes larger with increasing V_g (or N_S). Therefore a large portion of the conduction electrons, i.e., $\exp(-L/\ell_e)$, travel one side of the SL ballistically.

Plotted in Fig. 3 are the values of $\Delta\sigma_{2D}(B=0)$, extracted by the fast Fourier transform FFT method,[14] as a function of N_S for the SI devices fabricated using the samples 1–4 epiwafers (L=1.7 and 1.5 μm for samples 1 and 2, respectively, and L=1.8 μm for samples 3 and 4). We indeed see that $-\Delta\sigma_{2D}(B=0)$ oscillates with N_S, where we observe several nodes. Using the α vs N_S relations that are obtained from the WAL analysis of an unpatterned QW sample and a $\mathbf{k}\cdot\mathbf{p}$ model calculation using appropriate boundary conditions as discussed below, we can obtain α values at these node positions. We then can calculate θ values there using the relation $\theta=2\alpha m^*L/\hbar^2$.[15] In this way, we can assign θ values that satisfy $A(\theta)=0$ ($\theta\approx\pm0.4245\pi$, $\pm0.822\pi$, or $\pm1.178\pi$) to these node positions.

One might wonder why the shapes of the oscillations in Fig. 3 are rather deformed compared to the theoretical plot of $A(\theta)$. There are two reasons for this. First, the value of σ_{2D}

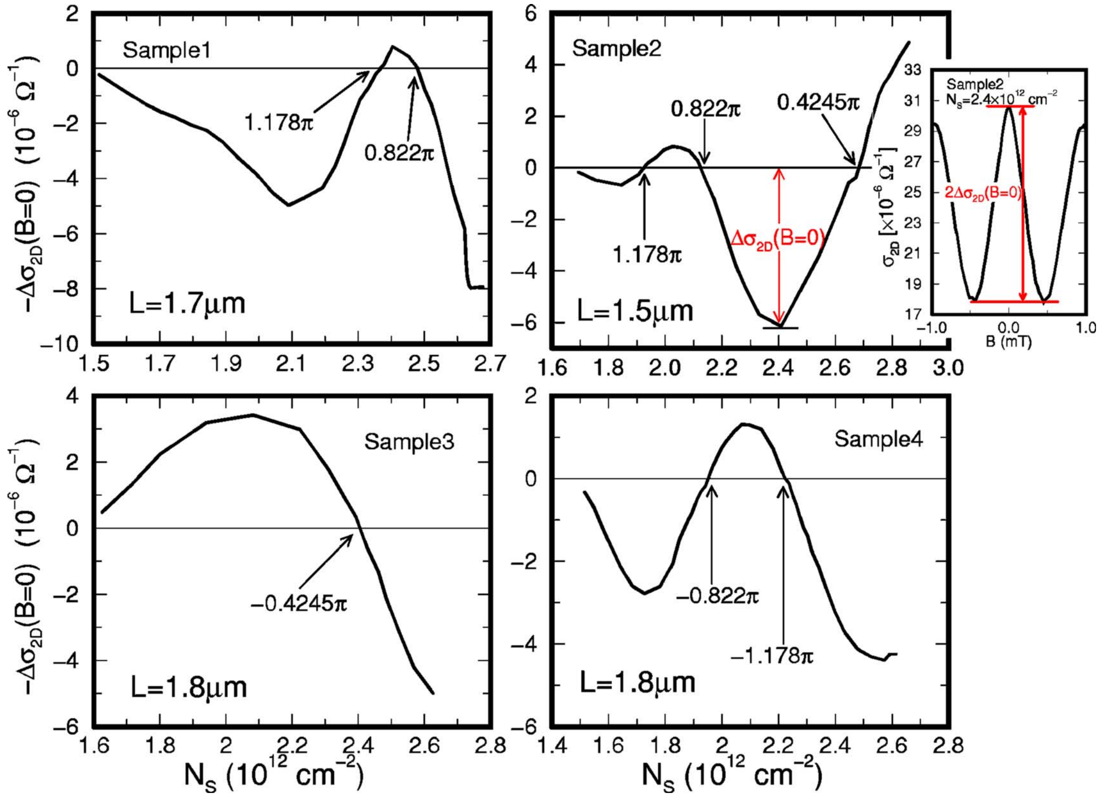

FIG. 3. (Color online) Amplitudes of the experimental AAS oscillations at $B=0$, plotted as a function of the sheet carrier density N_S, for various SL array samples ($L=1.5-1.8$ μm using the samples 1–4 epiwafers introduced in Ref. 10). The inset to the graph for sample 2 shows the relation between $\Delta\sigma_{2D}(B=0)$ and σ_{2D} for $N_S=2.4\times10^{12}$ cm^{-2}. The assigned θ values at the node positions are also given. We plot $-\Delta\sigma_{2D}(B=0)$ instead of $\Delta\sigma_{2D}(B=0)$ to match the signs of the values with those for $A(\theta)$ [Eq. (1)].

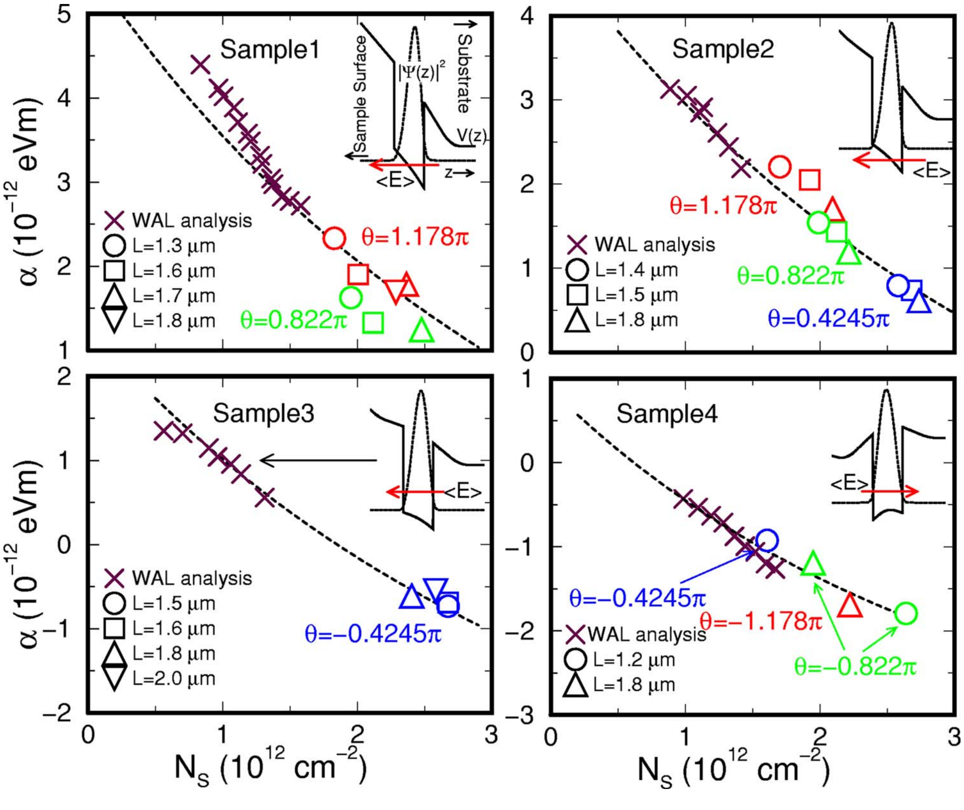

FIG. 4. (Color online) The values of the Rashba spin-orbit parameter α, for four different epiwafers denoted as samples 1–4 in Ref. 10, deduced from the three independent analyses: (1) the weak antilocalization analysis (crosses), (2) the analysis of the node positions in the $-\Delta\sigma_{2D}(B=0)$ vs N_S relations for the square loop arrays using the relation $\alpha=\theta\hbar^2/2m^*L$ (various symbols), and (3) the $\mathbf{k}\cdot\mathbf{p}$ model calculations using appropriate boundary conditions (dashed curves). The background impurity densities (N_i) assumed for the $\mathbf{k}\cdot\mathbf{p}$ calculations are $N_i=1\times10^{16}$, 4×10^{16}, 1.4×10^{16}, and 1×10^{16} cm^{-3} for samples 1–4, respectively. The insets to the figures show the direction of the built-in electric field $\langle E\rangle$ within the quantum well for each epiwafer.

decreases rapidly with decreasing N_S because of the reduction in the screening effect for the ionized impurity scattering. Then, the amplitude of the AAS oscillation is also reduced as the nature of electron transport becomes more and more diffusive. Second, our recent analysis showed that the inclusion of the Dresselhaus spin-orbit term, relevant to the bulk inversion asymmetry, in our SI model improves the agreement between the theoretical and experimental results. Detailed research along this line is currently under way.

It is a pedagogical exercise to calculate the α values at these node positions using the relation $\alpha = \theta\hbar^2/2m^*L$ ($\theta \approx \pm 0.4245\pi$, $\pm 0.822\pi$, or $\pm 1.178\pi$). In Fig. 4, we plot the α values obtained in this way (denoted as α_{SI}) for various SL array samples made of the samples 1–4 epiwafers as a function of N_S. Also plotted in Fig. 4 are (1) the α values obtained from the WAL analysis of unpatterned Hall bars (denoted as α_{WAL}) and (2) those obtained from the $\mathbf{k}\cdot\mathbf{p}$ model calculations (denoted as $\alpha_{\mathbf{k}\cdot\mathbf{p}}$) using the appropriate boundary conditions and assuming the presence of background impurities. We note that the unpatterned Hall bars for α_{WAL} were prepared on the same wafer pieces as those used for the SL array samples. We also note that we previously obtained $\alpha_{\mathbf{k}\cdot\mathbf{p}}$ values without assuming background impurities and found quantitatively good agreement with α_{WAL} values.[10] In the present work, however, we included the effect of the background impurities (mostly they are present in the $In_{0.52}Al_{0.48}As$ buffer layer) in the model calculation of $\alpha_{\mathbf{k}\cdot\mathbf{p}}$ to better fit the experimental α_{WAL} and α_{SI} values. It turned out that the values of the background impurity densities obtained from these fittings are reasonably small (typically 1×10^{16} cm^{-3}). It is recalled that negative α values assigned for samples 3 and 4 mean that the direction of the built-in electric field within the QW (denoted as $\langle E \rangle$) is opposite to those for samples 1 and 2 (see the insets in Fig. 4). For sample 3, the direction of $\langle E \rangle$ can be switched through the control of the applied gate voltage.

In summary, we demonstrated experimentally the electron spin interference phenomena based on the Rashba effect that were predicted previously.[11] For this demonstration, we prepared nanolithographically defined square loop array structures in $In_{0.52}Al_{0.48}As/In_{0.53}Ga_{0.47}As/In_{0.52}Al_{0.48}As$ quantum wells using the EBL and ECR dry etching techniques and measured the low-field magnetoresistances (**B** perpendicular to the sample surface) at low temperatures (0.3 K). We observed Al'tshuler-Aronov-Spivak oscillations, whose amplitudes at $B=0$ oscillated as a function of the gate voltage as a result of the spin interference. We also deduced the α values (Rashba spin-orbit coupling constant) from analysis of the spin interferometry experiments. We obtained quantitative agreement among (1) the α values obtained from the spin interferometry experiments, (2) those obtained from the weak antilocalization analysis, and (3) those obtained from the $\mathbf{k}\cdot\mathbf{p}$ model calculations.

---

*Present address: Graduate School of Information Science and Technology, Hokkaido University, Sapporo 060-0814, Japan. Electronic address: koga@ist.hokudai.ac.jp

†Present address: Graduate School of Engineering, Tohoku University, Sendai 980-8579, Japan.

[1] D. Awschalom, N. Samarth, and D. Loss, *Semiconductor Spintronics and Quantum Computation* (Springer-Verlag, Berlin, 2002).

[2] S. Datta and B. Das, Appl. Phys. Lett. **56**, 665 (1990).

[3] T. Koga, J. Nitta, H. Takayanagi, and S. Datta, Phys. Rev. Lett. **88**, 126601 (2002).

[4] J. Nitta, F. E. Meijer, and H. Takayanagi, Appl. Phys. Lett. **75**, 695 (1999).

[5] D. Bercioux, M. Governale, V. Cataudella, and V. M. Ramaglia, Phys. Rev. Lett. **93**, 056802 (2004).

[6] Y. K. Kato, R. C. Myers, A. C. Gossard, and D. D. Awschalom, Appl. Phys. Lett. **86**, 162107 (2005).

[7] E. I. Rashba, Fiz. Tverd. Tela (Leningrad) **2**, 1224 (1960) [Sov. Phys. Solid State **2**, 1109 (1960)].

[8] Y. A. Bychkov and E. I. Rashba, J. Phys. C **17**, 6039 (1984).

[9] J. Nitta, T. Akazaki, H. Takayanagi, and T. Enoki, Phys. Rev. Lett. **78**, 1335 (1997).

[10] T. Koga, J. Nitta, T. Akazaki, and H. Takayanagi, Phys. Rev. Lett. **89**, 046801 (2002).

[11] T. Koga, J. Nitta, and M. van Veenhuizen, Phys. Rev. B **70**, 161302(R) (2004).

[12] B. L. Al'tshuler, A. G. Aronov, and B. Z. Spivak, JETP Lett. **33**, 94 (1981).

[13] G. J. Dolan, J. C. Licini, and D. J. Bishop, Phys. Rev. Lett. **56**, 1493 (1986).

[14] Y. Sekine, T. Koga, and J. Nitta (unpublished).

[15] For example, we obtain $\theta \approx 0.965\pi$, 0.822π, and 0.4617π (from left to right) at the node positions for sample 2 in Fig. 3.